ACS OMEGA

http://pubs.acs.org/journal/acsodf

Article

Bioinspired NiO Nanospheres: Exploring *In Vitro* Toxicity Using Bm-17 and *L. rohita* Liver Cells, DNA Degradation, Docking, and Proposed Vacuolization Mechanism

Prashant B. Chouke, Ajay K. Potbhare, Nitin P. Meshram, Manoj M. Rai, Kanhaiya M. Dadure, Karan Chaudhary, Alok R. Rai,* Martin F. Desimone, Ratiram G. Chaudhary,* and Dhanraj T. Masram*

Cite This: *ACS Omega* 2022, 7, 6869−6884

Read Online

ACCESS | Metrics & More | Article Recommendations

ABSTRACT: The present work demonstrated a novel *Cleome simplicifolia*-mediated green fabrication of nickel oxide nanoparticles (NiO NPs) to explore *in vitro* toxicity in Bm-17 and *Labeo rohita* liver cells. As-fabricated bioinspired NiO NPs were characterized by several analytical techniques. X-ray diffraction (XRD) revealed a crystalline face-centered-cubic structure. Fourier transform infrared spectroscopy (FTIR), ultraviolet−visible diffuse reflectance spectroscopy (UV-DRS), Raman spectroscopy, and X-ray photoelectron spectroscopy (XPS) confirmed NiO formation. The chemical composition was confirmed by energy-dispersive X-ray spectroscopy (EDS) and X-ray photoelectron spectroscopy. Brunauer−Emmett−Teller (BET) revealed the mesoporous nature. Scanning electron microscopy (SEM) and transmission electron microscopy (TEM) revealed the formation of 97 nm diameter nanospheres formed due to the congregation of 10 nm size particles. Atomic force microscopy (AFM) revealed the nearly isotropic behavior of NiO NPs. Further, a molecular docking study was performed to explore their toxicity by binding with genetic molecules, and it was found that the docking energy was about −9.65284 kcal/mol. On evaluating the *in vitro* toxicity of NiO NPs for Bm-17 cells, the study showed that when cells were treated with a high concentration of NPs, cells were affected severely by toxicity, while at a lower concentration, cells were affected slightly. Further, on using 50 μg/mL, quick deaths of cells were observed due to the formation of more vacuoles in the cells. The DNA degradation study revealed that NiO NPs are significantly responsible for DNA degradation. For further confirmation, trypan blue assay was observed for cell viability, and morphological assessment was performed using inverted tissue culture microscopy. Further, the cytotoxicity of NiO NPs in *L. rohita* liver cells was studied. No toxicity was observed at 1 mg/L of NiO NPs; however, when the concentration was 30 and 90 mg/L, dark and shrank hepatic parenchyma was observed. Hence, the main cause of cell lysis is the increased vacuolization in the cells. Thus, the present study suggests that the cytotoxicity induced by NiO NPs could be used in anticancer drugs.

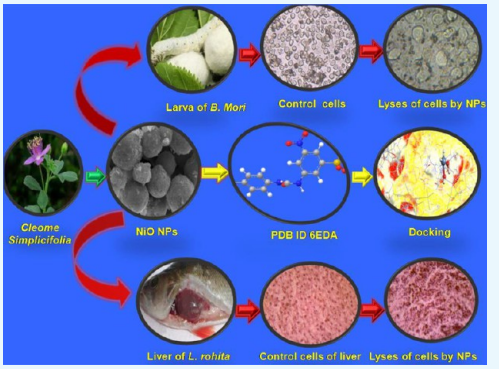

INTRODUCTION

Bioinspired nanomaterials have attracted incredible attention in the field of nanoscience and nanotechnology and have been employed in several applications including biomedical, drug delivery, clinical, bioengineering, cosmetics, agriculture, catalysis, aerospace engineering, energy storage, solar cells, environmental remediation, and textiles.[1,2] Despite their vast utilization in various fields, some bioinspired nanomaterials have shown toxic effects on human beings, insects, aquatic life, and the environment, which led to the origin of a new discipline called "Nanotoxicology". Currently, more attention is paid to the toxicity of nanoparticles that could have been generated from civilization and industrialization. The different industrial processes result in the production of toxic nanomaterials like heavy metal nanoparticles, metal oxide nanoparticles, nanocomposites, nanopolymers, and carbon-based nanomaterials that harm the environment, aquatic life, insects, zooplankton, microorganisms, human health, and so forth.[3−8] At present, metal NPs, carbon materials, and carbon-based nanomaterials have attracted large attention and are being applied in various fields including biomedical applications.[9−13] But the carbon-based nanomaterials are the ones that are strongly ruining the atmosphere by aerial emission, spills, and storm-water runoff from land to surface waters that cause

Received: November 20, 2021
Accepted: February 10, 2022
Published: February 21, 2022

toxicity to aquatic life. Moreover, some metal oxide nanoparticles (NPs) are also more hazardous materials, and their toxicity is measured based on the concentration, particle size, structural morphology, surface area, and porosity.[14,15] Primarily, the lower the concentration of toxic materials in the aqua system is, the higher is the growth of aquatic organisms,[16] while a higher concentration induces toxicity to the aquatic life.[17] There are several toxic metal oxide NPs like Li_2O, BeO, PbO, Al_2O_3, SnO, As_2O_4, Tl_2O_3, PoO_2, CrO_3, Fe_2O_3, CuO, CdO, HgO, and NiO. These have no biological role in human/organism life; instead, these are noxious to the life cycle of all the organisms. Therefore, these are not recommended for medical appliances. However, due to their ultra-small sizes, they can easily enter the human body, insects, and aquatic animals and may rapidly contact with the most sensitive organs like the liver, kidney, lungs, hearts, brain, spleen, etc. Among metal oxide NPs, NiO NPs are one of the highly toxic nanomaterials that can be synthesized by conventional and green-assisted methods. Several reports were published on NiO NPs by various groups using conventional techniques; however, only few reports were *published* by phytosynthesis method. For instance, the leaf extract of *Geranium wallichianum* was reported by Abbasi *et al.*,[18] fresh leaf extract of *Rhamnus triquetra* by Iqbal *et al.*,[19] leaf extract of *Rhamnus virgata* by Iqbal *et al.*,[20] leaf extract of *Berberis balochistanica* by Uddin et al.,[21] *Hordeum vulgare* by Din *et al.*,[22] extract of tragacanth by Sabouri *et al.*,[23] *Pinus roxburghii* by Mirza *et al.*,[24] seed extract of *Lactuca serriola* by Ali *et al.*,[25] peel-waste of rambutan by Yuvakkumar *et al.*,[26] okra plant extract by Ghazal *et al.*,[27] *Zingiber officinale/Allium sativum* by Haider *et al.*,[28] extract *of Agathosma betulina* by Thema *et al.*,[29] Arabic gum by Sabouri *et al.*,[30] and leaf extract of *Aegle marmelos* by Ezhilarasi *et al.*[31] According to the literature study, this is the first report of *Cleome simplicifolia*-mediated phytosynthesis of NiO NPs. Moreover, our group has reported various bioinspired metal/metal oxide-based nanomaterials for different biomedical applications.[32−35]

NiO NPs are one of the highly toxic nanomaterials that can alter the water quality and ultimately are hazardous to organisms and human beings, too. Also, NiO NPs are rated as a human carcinogen by the World Health Organization. Recently, few reports on NiO NPs revealed their high toxicity especially for bacteria, aquatic life, and maize seedlings.[36−42] Moreover, in mammalian systems, the toxic effects of NiO NPs have been explored mainly on the airway cells,[43−45] lung, liver, and inflammation in tracheal instillation in rats.[46,47] As per the toxicity mechanism of NiO NPs, nanoparticles can bind with the cell components like sulfhydryl, carboxyl, or imidazole groups of proteins and alter their activities. Interference with cellular processes often causes redox imbalances and stress in metal-exposed organisms. The ability of NiO NPs to cause genotoxic effects in DNA damage by generating reactive oxygen species (ROS) is a key factor. ROS includes the singlet oxygen (O_2), hydroxyl radical ($OH^{\cdot}$), superoxide radical ($O_2^{\cdot-}$), hydroperoxyl radical ($HO_2^{\cdot}$), hydrogen peroxide (H_2O_2), and carbonyl (RO). ROS can attack virtually all macromolecules, which results in serious damage to cellular components. ROS is also considered as the main underlying chemical process in nanotoxicology, leading to secondary processes that can cause cellular damage and eventually cell death. Indeed, there are several reports on the cytotoxicity and apoptosis induced by NiO NPs on the life cycle of human beings, plants, insects, fishes, and so forth.[41,48] Nevertheless, vacuolization is also one of the causes of cells death, which is induced by an overload of toxic endocytosis.[49] Ultimately, DNA and many other cellular organelles could be damaged by more vacuolization.[50] Many insects and fish are daily becoming a victim of the cytotoxic effects of NiO NPs that are released from industries, electronic products, waste garbage, and domestic wastewater.

Several insects and fishes are very precious for economic development and as human food sources. One of them is silk moth (*Bombyx mori*), and another is the *Labeo rohita* fish. *B. mori* is an economically important insect. *B. mori* is a domestic silk moth, an insect from the moth family Bombycidae. It is the closest relative of *Bombyx mandarina*, the wild silk moth. The silkworm is the larva or caterpillar of a silk moth. It is an economically important insect, being a primary producer of silk. Domestic silk moths are entirely dependent on humans for reproduction as a result of being commercially viable in the production of silk.[51] Insect cells are now routinely used to produce higher eukaryotic proteins using baculovirus expression systems, as they can modify the proteins co-translationally and post-translationally including glycosylation, phosphorylation, and protein processing, similar to mammalian cells. Currently, there are two baculovirus-based expression systems used for producing recombinant proteins: the *Autographa californica* multicapsid nucleopolyhedrovirus, which infects Sf9/Sf21 cells and *Trichoplusia ni* larvae, and the *B. mori* nucleopolyhedrovirus (BmNPV), which infects *B. mori* cells and larvae. Recent reports indicated that protein expression using silkworm or its pupae is 10- to 100-fold higher than that using *B. mori* cells.[52] However, efficient and BmNPV-susceptible *B. mori* cell lines are required to generate a large quantity of resulting recombinant viral stocks to inoculate silkworm larvae for protein production.[53] Although several *B. mori* cell lines derived from embryos and larval and pupal ovaries[54−56] are available, there is a constant need to develop newer cell lines to replace the commonly used cell lines because the macula-like virus has been identified in BmN cells.[56]

Likewise, *L. rohita* (Rohu fish) is extensively utilized in aquaculture and is a common food of northern, central, and eastern countries like Nepal, Bangladesh, Pakistan, Sri Lanka, Myanmar, Vietnam, and India. Rohu fishes are abundantly found in India in several water bodies like wetlands, puddles, canals, streams, ponds, lakes, rivers, oceans, seas, etc. But the release of toxic ultra-small nanoparticles due to increasing industrialization demolishes insect and aquatic life. Keeping this perspective, to probe the toxicity of nanoparticles on the life cycle of insects and aquatic, we had selected *Bombyx mori* (*B. mori*) and *Labeo rohita* (*L. rohita*) fishes in the present study to investigate the toxicity of bioinspired NiO nanospheres. Furthermore, as per the literature survey, there are no reports available on the toxicity of NiO nanospheres on *L. rohita* and *B. mori*.

In the present work, we have studied the *in vitro* toxicity of bioinspired NiO NPs on the proliferation of the *B. mori* cell line (Bm-17 cells) and liver cells of *L. rohita* fish. Further, cell viability was determined by trypan blue assay, necrotic cell morphology, and DNA damage by agar gel-electrophoresis. Astonishingly, we are reporting for the first time a massive vacuolization induced by NiO NPs on the insect cell line (Bm-17 cells). To the best of our knowledge, this is the first report that demonstrates the cytotoxicity of NiO NPs *via* single

https://doi.org/10.1021/acsomega.1c06544
ACS Omega 2022, 7, 6869−6884

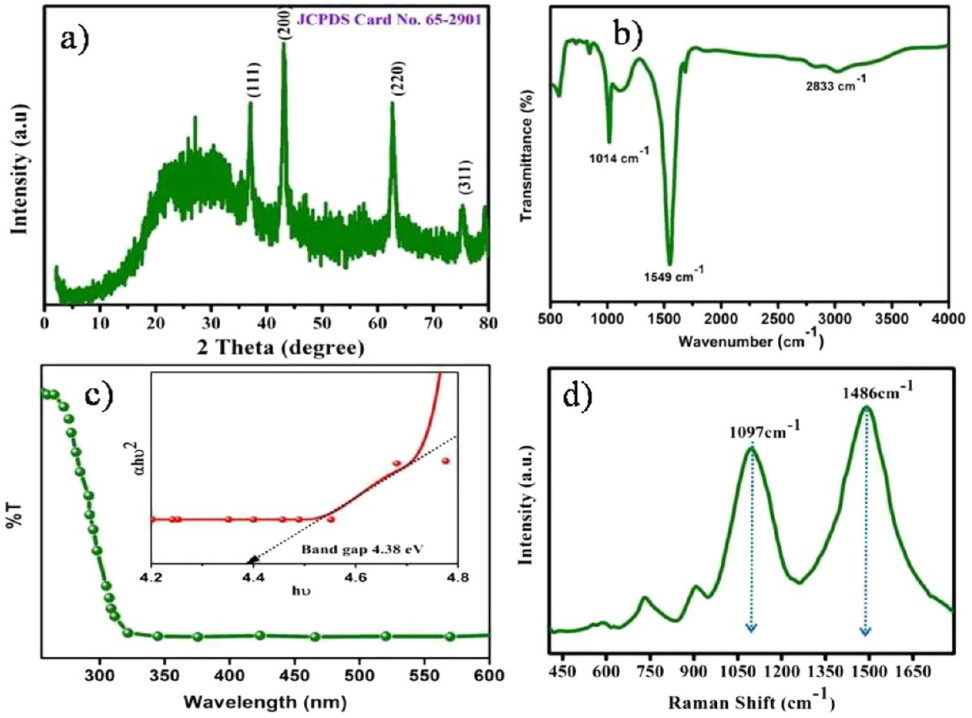

Figure 1. (a) XRD pattern, (b) FTIR spectrum, (c) DRS with band gap, and (d) Raman spectrum of NiO NPs.

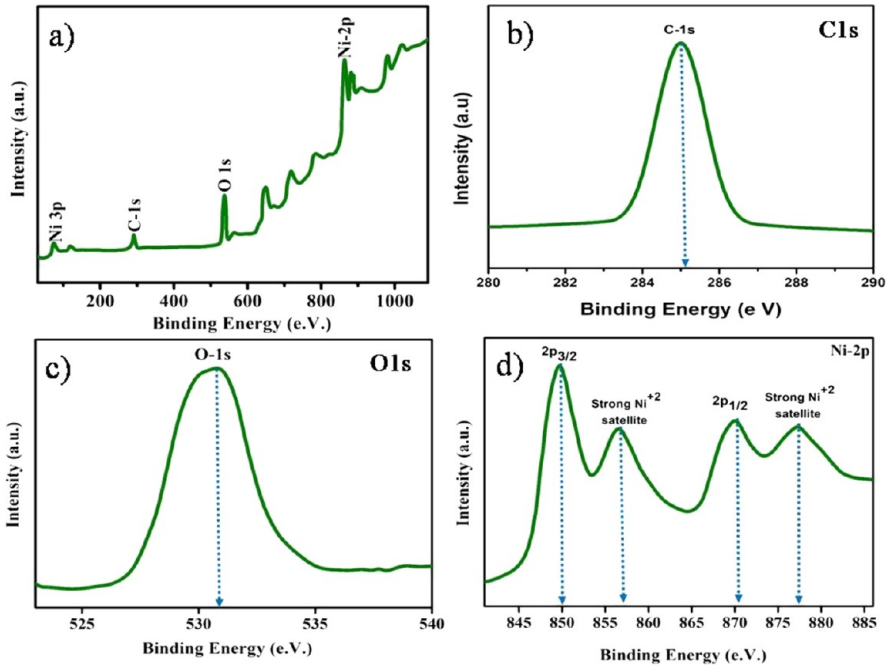

Figure 2. XPS of NiO NPs: (a) survey, (b) C 1s, (c) O 1s, and (d) Ni 2p of NiO NPs. Furthermore, the surface area and porosity of biosynthesized nanomaterials were investigated by BET (Figure 3b). The specific surface area of the NiO powder was found to be 44 m^2/g, while its average pore diameter was found to be 4.7 nm; therefore, it was found to be a mesoporous type material. Moreover, the pore size distribution curve revealed the monodispersed nature of particles. Hence, these properties advocated that the material could be used as a good adsorbent and in a toxicity study. The obtained results were perfectly matched with the previously reported study.[66]

oxygen DNA degradation, which induced cytotoxicity in DZNU-Bm-17 cells and liver cells of *L. rohita* fish.

RESULTS AND DISCUSSION

Structural Confirmation of Biosynthesized NiO NPs. An XRD study was performed to investigate the crystallinity and structure of biosynthesized NiO NPs, and the obtained XRD pattern is shown in Figure 1a. The XRD pattern of NiO NPs exhibited sharp peaks at 2θ = 37.1, 43.1, 62.7, and 75.2° that correspond to (111), (200), (220), and (311) crystal planes, respectively. The hkl plane values revealed that NiO NPs have a face-centered-cubic (FCC) structure (JCPDS file no. 65-2901).[57,58] A well-defined sharp peak indicates the higher crystallinity of the synthesized NiO NPs. Hence,

https://doi.org/10.1021/acsomega.1c06544
ACS Omega 2022, 7, 6869−6884

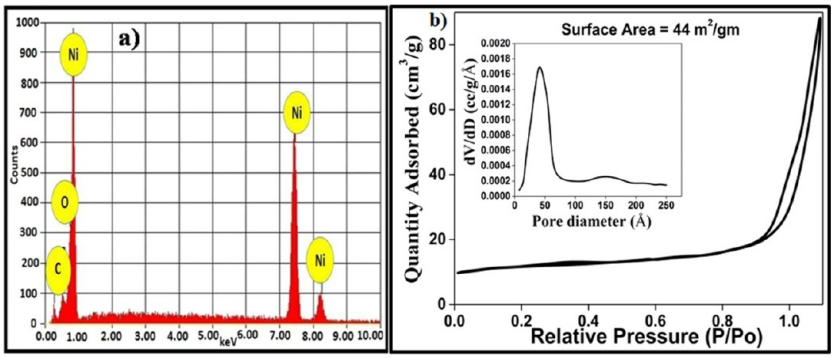

Figure 3. (a) EDS spectrum and (b) nitrogen adsorption−desorption isotherm of NiO NPs with pore size distribution curve as the inset.

crystallite sizes of NPs were estimated using the Debye−Scherrer formula. The average crystallite size of NPs was estimated to be 7 nm.

Further, chemical bonding was validated using FTIR spectroscopy, and the spectrum obtained is shown in Figure 1b. The band at 589 cm^{-1} can be assigned to Ni−O chemical bonding. A weak peak was observed in the spectrum at 549 and 3033 cm^{-1}, which can be ascribed to H−O−H bending and −OH stretching vibrations that can be due to the presence of atmospheric water during analysis. The peak positioned around 2833 cm^{-1} was spotted for the $-CH_2$ group, which might be due to plant extract residue.[59]

Then the sample was examined by UV-DRS spectroscopy to seek out the electronic property (Figure 1c). The NiO NPs exhibited an absorption band at 275 nm that indicated the formation of NPs; hereafter, the absorbance decreases around 280−320 nm, indicating the nucleation, growth, and reduction of particle sizes because of the biogenic surfactant. The band gap energy of biosynthesized NiO NPs was estimated by a Kubelka−Munk (K−M) plot (Figure 1c inset). The NiO material corresponds to p-type semiconductors, and therefore its bandgap (Eg) was found to be high. The estimated bandgap Eg = 4.38 eV was equivalent to that of reported NiO NPs.[60] The augmentation in Eg might be due to the reduction in particle sizes of NiO.[61]

The chemical and structural bonding was studied by Raman spectroscopy. The Raman spectrum of NiO NPs (Figure 1d) exhibited three second-order phonon modes and one 2M mode. The second-order phonon modes were observed at 730.8, 905.8, and 1094.3 cm^{-1}, which can be attributed to 2TO, LO + TO, and 2LO modes, respectively (where TO is transverse optical and LO is longitudinal optical). A peak with the highest intensity observed in the spectrum at 1486 cm^{-1} is attributed to the 2M (double magnon scattering) mode. Considering the Raman shift difference that is inferred to size or strain/stress effects, the position and relative intensities of the peaks are in good agreement with the reported values of the NiO phase.[62,63] Moreover, the chemical composition and oxidation state of the prepared NiO NPs sample were explored by the XPS (Figure 2a−d). The XPS survey spectra of the sample showed the peaks for the nickel (Ni), oxygen (O), and carbon (C) atoms confirming the presence of main elements as Ni, O, and C (Figure 2a). In the C 1s spectrum, the analogous peak obtained at 285.1 eV can be attributed to the presence of adventitious carbon contamination (Figure 2b), while the peak observed at 531.7 eV in the O 1s core spectrum corresponds to the M−O bonding, which confirms the existence of O^{2-} (Figure 2c). In the Ni 2p core spectrum, the peaks observed at 850.0 and 871.0 eV confirmed the formation of NiO, while two discrete strong satellites peaks were observed at 857.2 and 977.3 eV that corresponded to Ni $2p_{3/2}$ and Ni $2p_{1/2}$ spin−orbit components, which revealed that Ni is in a +2 oxidation state (Figure 2d). Thus, these XPS results confirmed the synthesis of biosynthesized black color NiO.[64] Next, the presence of elements, chemical composition, and purity of the sample were verified by EDS (Figure 3a). Noteworthily, EDS spectra show the existence of NiO and contain peaks for Ni, O, and C elements. However, no traces of other elements were found except carbon, thus confirming the purity of NiO NPs. As well, it was in good agreement with the XRD study, and this confirmed the purity of NiO NPs.[65]

Morphology Investigation of NiO NPs. The surface morphology, particle sizes, and structure of cubic phase NiO NPs were investigated by SEM, TEM, and AFM techniques. The SEM images (Figure 4) displayed the spherical shape of

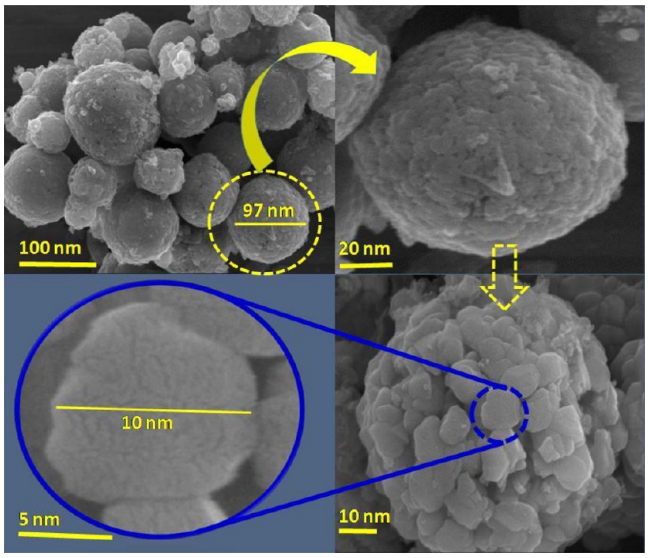

Figure 4. SEM images of NiO NPs.

particles like a nanoball with a diameter in the range of 97 nm. All nanospheres were nearly identical in shape and size. These nanospheres were developed by the congregation of numerous nanoscale particles with a size of 10 nm (Figure 4).[67]

The nanocrystals preferred to aggregate into a nanospherical shape. Figure 4 shows the presence of numerous nanospheres on the surface of a nanoball that were observed due to aging time. With the increase of aging time, the size of the

https://doi.org/10.1021/acsomega.1c06544
ACS Omega 2022, 7, 6869−6884

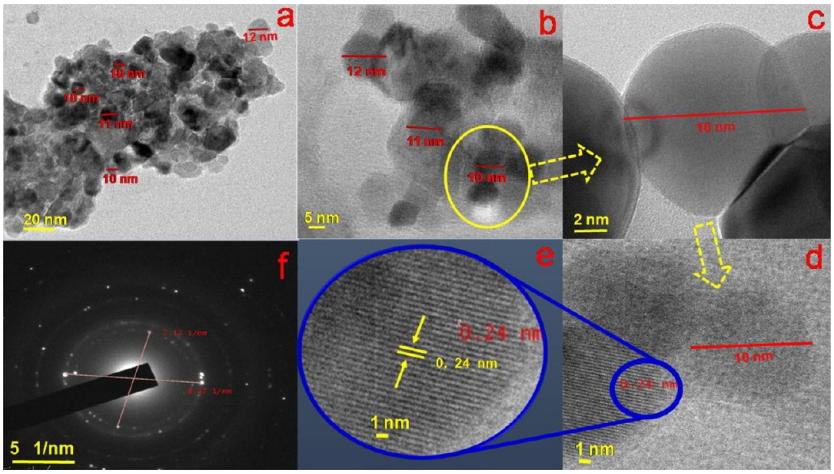

Figure 5. (a–e) TEM micrographs and (f) SAED pattern of NiO NPs.

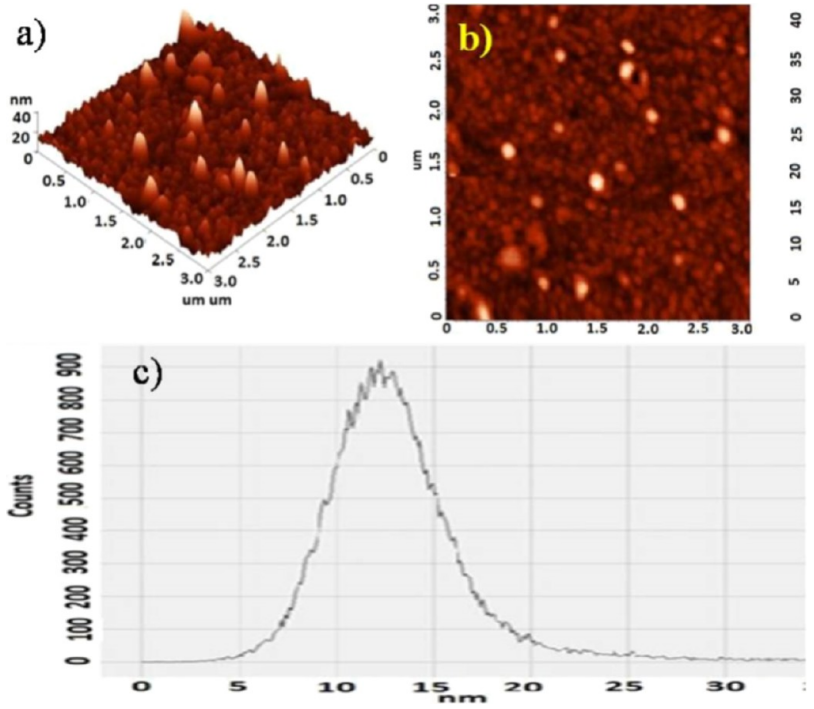

Figure 6. NiO NP images: (a) 3D AFM, (b) 2D AFM, and (c) AFM histogram graph.

nanospheres gradually decreases (Figure 4). The development of uniform minimally agglomerated spheres is because of homogeneous nucleation with constant and prolonged heating at a higher temperature. In contrast, in the conventional heating mode, the time for nucleation might be sufficient but varied heat zones led to the formation of bigger particles and wider distribution. Hence, owing to the reliable uniformity in size, shape, and mass, the biosynthesized materials are called homogenized nanomaterials. The homogenization or near monodispersity in the nanospheres might be due to the role of the biogenic surfactant and stabilizing agents during the synthesis.[68] Subsequently, the biosynthesized NiO sample was explored by TEM to estimate the particle sizes and shapes (Figure 5a–d). TEM micrographs clearly show that the nanoparticles are of nearly uniform size with a spherical shape and an average diameter of 10 nm (Figure 5a). Moreover, from the TEM micrographs, it was revealed that the crystalline nanoparticles appeared to be quantum dot sized and associated with bio-extract sheets. Most significantly, we succeeded in generating uniform single-crystalline nanoparticles. According to earlier reports, researchers also succeeded in developing single-crystalline nanoparticles with a spherical shape.

In the present study, we were successful in fabricating single-nanocrystalline spheres of NiO, and further, these NPs aggregated to generate a single sphere of a larger size. Homogeneity particularly in shape and sizes was attained, and the distinctive lattice fringes were examined in the HR-TEM image (Figure 5c–e).[69] The SAED pattern shown in Figure 6f shows bright spots that confirm the crystallinity of as-synthesized NiO NPs, supporting the XRD results. The average crystalline size of cubic NiO NPs was estimated to be around 6 nm by the Debye–Scherrer equation using XRD data. Importantly, in the present work, the capping and reducing agent, which was a plant extract, played a key role in

https://doi.org/10.1021/acsomega.1c06544
ACS Omega 2022, 7, 6869–6884

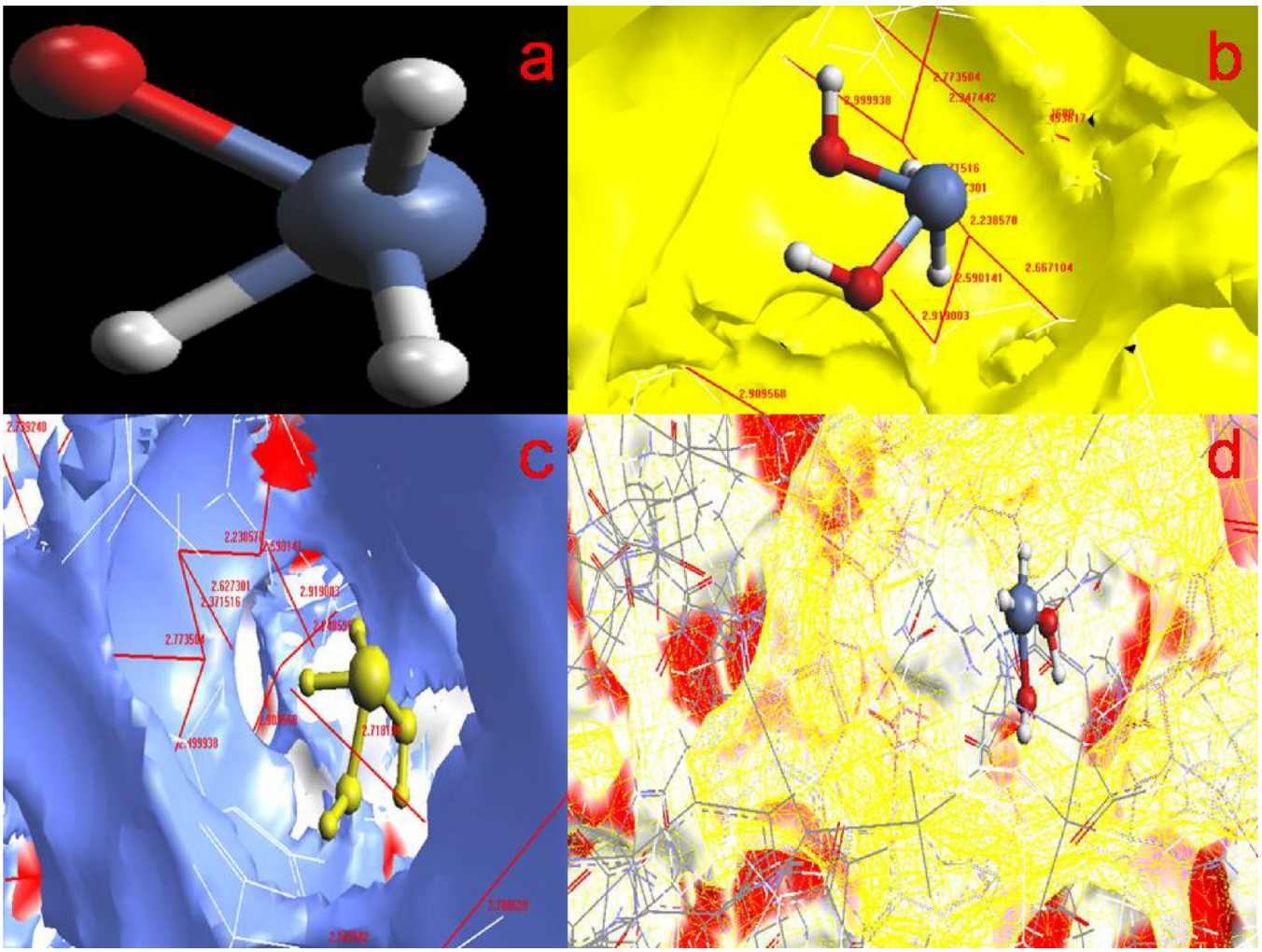

Figure 7. The molecular docking investigation of NiO NPs: (a) 3D ball and stick model of nanosphere NiO NPs, (b) 3D ball/stick model of nanosphere NiO NPs fitted at the center of the protein (PDB ID 6EDA), and (c, d) ligand docked with the protein surrounded with different hydrogen bonding residues.

the formation of nearly uniform sized NPs. Moreover, atomic force microscopy (3D and 2D images) of the material suggested a fine surface roughness, while the AFM histogram shows a nearly monodisperse nature and particle sizes of around 12−14 nm (Figure 6a−c). XRD and AFM study revealed nanoscale materials with a nearly isotropic behavior of particles. After the structural and morphological evaluation of the biosynthesized nanomaterial, it was employed to evaluate cytotoxicity interaction with insect cells and liver cells of *L. rohita* fishes owing to its high specific surface area with a mesoporous structure. It is coherent to state that the binding of particles to microorganisms depends on the nano/micro sizes and their surface. NPs have a larger surface area with a mesoporous structure, which could enhance the interaction with biological motifs; therefore, the bactericidal effect is enhanced due to the nanoscale sizes and higher surface area than the bulk one; hence, they impart more cytotoxicity to microorganisms.

Molecular Docking of NiO NPs. After the complete structural and morphological investigation of NiO NPs, an attempt is made to seek out the drug efficiency and inhibition ability of the newly biosynthesized material. It is one of the most important aspects to know the molecular interactions between materials (ligand) with a cell wall and organelles. Moreover, inhibition information between the ligand and receptor enzyme is most essential for the calculation of the probable binding energies. According to the literature reports, different metal oxide nanoparticles having better cytotoxicity activity with high binding energies were utilized as biomedicine for the treatment of various tumors and cancer cells and for the elimination of pathogens.[45,70,71] Keeping this perspective, in the present study, molecular docking of nanosphere NiO NPs was performed by replacing a natural inhibitor, 4-hydroxy-3-nitro-5-({[4-(trifluoromethyl) phenyl]carbamoyl}amino)-benzene-1-sulfonamide, to inhibit an enzyme, *i.e.,* PDB ID 6EDA.[72,73] Herein, a well-designed inhibitor (nanosphere NiO NPs) was docked with protein crystal structure PDB ID 6EDA (Figure 7). The finalized 3D structure of an inhibitor or ligand was tested for global minima by ascertaining the minimum energy values, and the calculated docking energy was about −9.65284 kcal/mol. From the calculated docking energy, it was revealed that considered NPs were more effective to explore their toxicity by binding with genetic molecules. Besides, different amino acid residues were docked with a ligand and showed good hydrogen bonding distances of 2.0 Å (Table 1). Thus, the docking investigation supported that bioinspired nanosphere NiO NPs can be utilized for *in vitro* cytotoxicity.

https://doi.org/10.1021/acsomega.1c06544
ACS Omega 2022, 7, 6869−6884

Table 1. Docking Study of Selected Amino Acids by NiO NPs

amino acid residues	hydrogen bond (Å)
613 VAL, 92 GLN, 199 THR	2.247175, 2.347442, 2.319003
121 VAL, 120 LEU, 199 THR	2.260512, 2.3715
92 GLN, 91 ILE	2.2343
119 HIS, 117 GLU	2.42946
118 LEV, 197 SER	2.24859
143 VAL, 142 ALA	2.247178

Table 2. Dose-Dependent Response to NiO NPs by MTT Colorimetric Assay

sr. no	dose of NiO NPs (μg)	MTT test mortality (mean ± SE)
1	0.5	23.6667 ± 1.201
2	1.0	44.6667 ± 1.881
3	1.5	74.333 ± 1.763
4	2.0	84.777 ± 1.154
5	3.0	92.000 ± 1.182

Evaluation of *In Vitro* Toxicity of NiO NPs. To examine *in vitro* cytotoxicity, the cells were treated with NiO NPs. The MTT assay was executed to determine the optimal dose, cell viability, and cytotoxicity of nanoparticles on Bm-17 cells (Figure 8a).[74,75] Normal B-17 cells were used as a control (Figure 8b). The Bm-17 cells' morphology was observed at different times and concentrations of NiO NPs. To examine the effect of NiO NPs on Bm-17 cells, an inverted tissue culture microscope with an attached high-resolution camera was used to observe the morphological changes (Figure 8c–i). Initially, the cells were treated with a lower concentration (0.5 μg/mL) of NiO NPs; next, the concentrations used were 1.0, 1.5, and 2.0 μg/mL for 1 h and then 3 μg/mL for 120 and 240 min. The lysis of cells was found to be between 22.33 ± 1.52 and 88.33 ± 3.511% (Table 2). As shown in Figure 8b, it refers to the proliferation of cells at zero hour or control cells. The cells were treated with a high concentration of NiO NPs and were affected severely by toxicity, while at a lower concentration, cells were affected slightly. A concentration of 2 μg/mL of NiO NPs caused a significant decrease in cells' viability (Figure 8h). The prominent reason for cell lyses may be the number of vacuoles formed in the cells (Figure 8c–h). As the number of vacuoles increases, the cells changed their shapes, cells shrinkages, blebbing, DNA fragmentation, and mRNA degradation, and wound to cytoplasmic organelles. Eventually, cytoplasmic organelles were evacuated from the cells. Hence, it was a programmed cell death, *i.e.,* apoptosis. The second well-known reason responsible for cells' death is apoptosis. Extensive apoptosis of cells at 3 μg/mL of NiO NPs was about 92.000 ± 1.182% (Figure 8b–h). Thus, NiO NPs can be considered as an effective nanotoxic material, and hence, the property of apoptosis in the cells by the NiO NPs shows that they can be exploited as anti-cancer candidates.[76]

Moreover, the apoptosis and morphological behavior of cells were observed by the treatment with 3 μg/mL NiO NPs at 10, 20, 30, 40, 50, 60, and 80 min, and the result shows a spike-like membrane, vesicle appearance in the cells, and changes in the cell shape (Figure 9). Trypan blue exclusion assay and morphological assessment under a phase contrast inverted microscope at different time intervals were performed, and the percentage (%) inhibition in growth was quantified. The

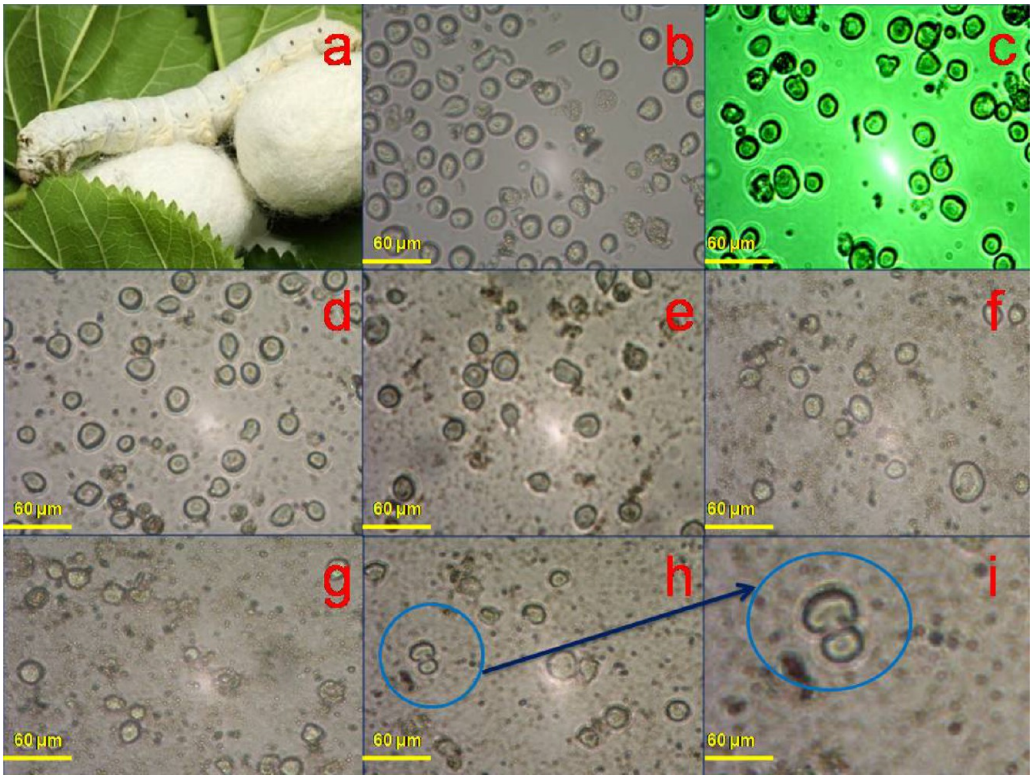

Figure 8. (a) Larva of *Bombyx mori silk moth*; (b) control cells of Bm-17; the vacuolization formation and cell lyses was occurred in Bm-17 cells due to (c) 0.5 μg mL/1 h; (d) 1.0 μg mL/1 h; (e) 1.5 μg mL/1 h; (f) 2.0 μg mL/1 h; (g) 3.0 μg mL at 120 min; and (h) 3 μg/mL at 240 min of NiO NPs; and (i) high resolution of 3 μg/mL at 240 min (it was observed under a phase contrast microscope, 10×).

https://doi.org/10.1021/acsomega.1c06544
ACS Omega 2022, 7, 6869−6884

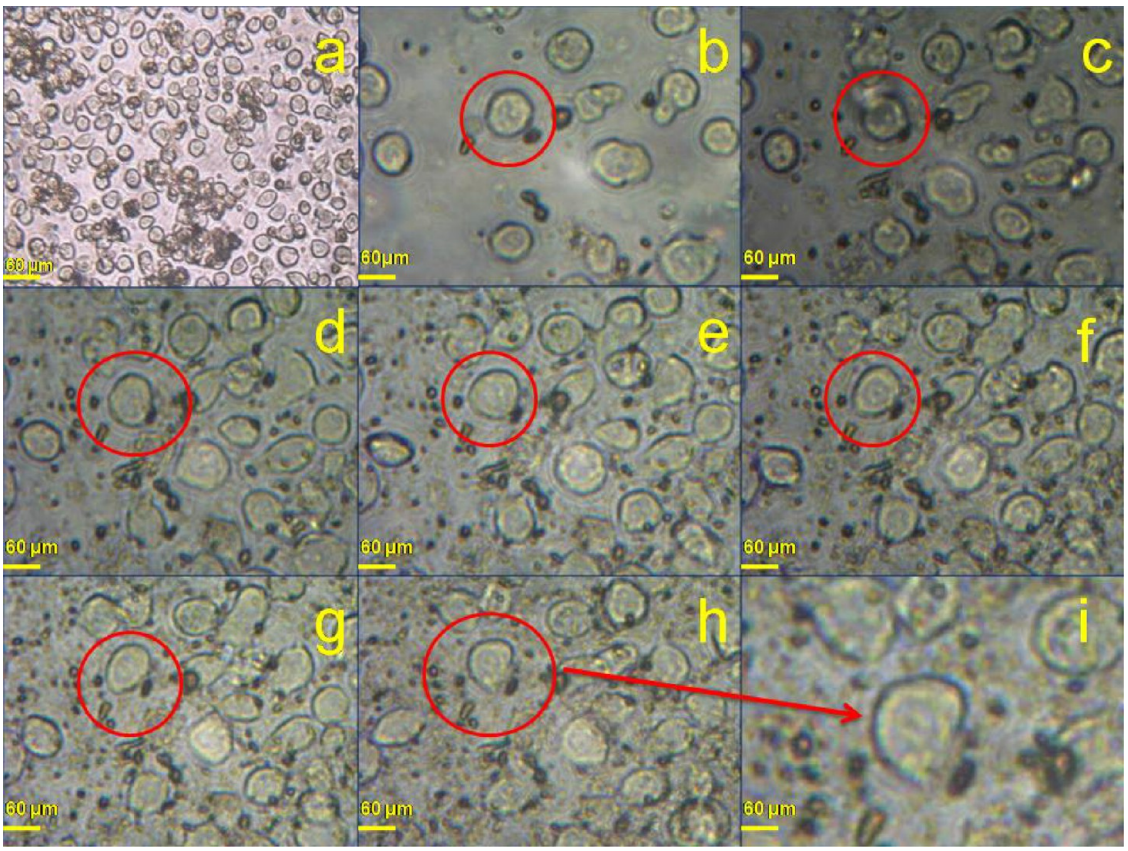

Figure 9. (a) Normal Bm-17 cells; and after a shot of 3 μg/mL NiO NPs in Bm-17 cells, apoptosis and morphological behaviors were observed at (b) 1 min, (c) 10 min, (d) 20 min, (e) 30 min, (f) 40 min, (g) 50 min, and (h) 80 min; (i) high-resolution image at 80 min (lyses of cell).

formation of vacuoles started in the cells after 10 min. The formations of numerous vacuoles by procaine and procainamide have also been reported earlier.[77] Endocytosis in eukaryotic cells is characterized by the continuous and regulated formation of membrane vesicles at the plasma membrane, and each of these vesicle types results in the delivery of its contents to lysosomes for degradation. The plausible mechanism of cell lyses by NiO NPs is shown in Figure 12.

It is assumed that the large cytoplasmic vacuoles developed due to the external pressure generated by NiO nanoparticles or membrane fusion of vesicles formed by the active endocytosis of NiO NPs. Further, the cells were treated with 3 μg/mL NiO NPs for 240 min, and an enhanced effect of nanoparticles' toxicity was detected (Table 3). Most of the cells were lysed at higher concentrations. However, when the cells were treated with 50 μg/mL, quick cell lyses were observed due to the more vacuoles formed in the cells (Figure 10).[14,15,49] Overall, the rapid death of the Bm-17 cells was caused by the vacuolization formed by NiO NPs.[78] Moreover, the observed toxicity could also be due to Ni cations leaching from the nanoparticles, but the current investigation did not explore this in detail.

Table 3. Growth Inhibition of Bm-17 Cells in 2 and 3 μg/mL of NiO NPs in DMSO

duration (min)	control	2 μg		3 μg	
in min	240 min	120 min	240 min	120 min	240 min
initial 10^4	50.25	155.5	25.25	64.75	62.25
final 10^4	33.5	57.5	14.2	52.25	9.25
difference%	66.66	63.03	44.32	19.31	85.15

Furthermore, to verify the protoplasmic degradation, a DNA degradation study was performed using NiO NPs. The DNA degradation by NiO NPs is shown in Figure 11a. The study revealed that NiO NPs are significantly responsible for DNA degradation. From Figure 11a, it is observed that there is no DNA degradation in lane 1 (control), lane 2 (DNA + supernatant + DMSO), and lane 3 (DNA + 25 μg NiO NPs). Similarly, in lane 4 (DNA + 4 mM sodium citrate), there is no DNA degradation observed. However, in lane 5 (DNA + 50 μg NiO NPs), lane 6 (DNA + 100 μg NiO NPs), lane 7 (DNA + 150 μg NiO NPs), and lane 8 (DNA + 200 μg NiO NPs), strong DNA degradation is observed in 2 h at 37 °C in the phosphate buffer saline solution maintained at pH 7.5. In lane 9 (DNA + 400 μg NiO NPs), a complete DNA degradation due to the high concentration of NiO NPs is observed. Hence, this study strongly revealed that NiO NPs are responsible for DNA degradation, and it may be due to the single oxygen mediated DNA damage.[6] Hence, it is confirmed that Bm-17 cells were lysed due to vacuolization developed by NiO NPs. Moreover, the effects of different concentrations of NiO NPs on vacuolization in Bm-17 cells were examined under an inverted tissue culture microscope (Figure 11b). Further, viability plots were drawn that reveal that treated Bm-17 cells were unexpectedly lysed in 4 h (Figure 11c). The percent inhibition in growth was quantified based on trypan blue dye exclusion assay at different times.

Cytotoxicity in Liver Cells of *L. rohita*. The cytotoxicity in liver cells of *L. rohita* fishes (Figure 13a) was also studied

https://doi.org/10.1021/acsomega.1c06544
ACS Omega 2022, 7, 6869−6884

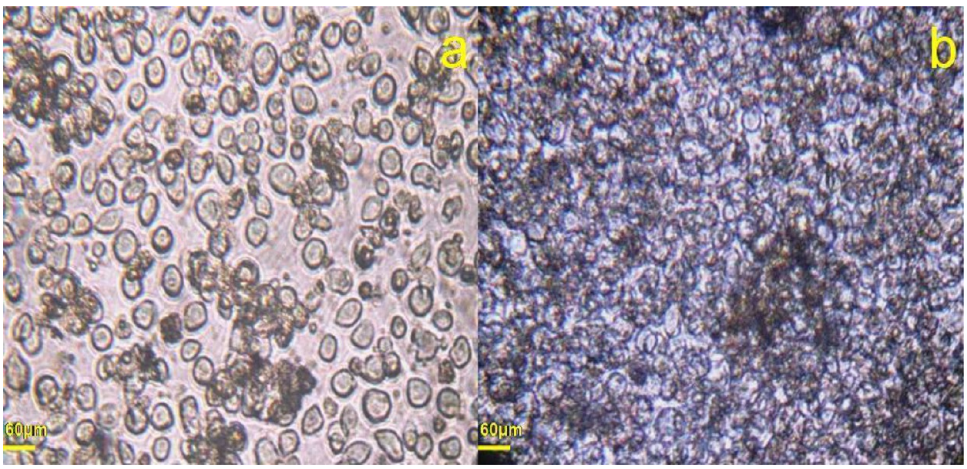

Figure 10. (a) Control Bm-17 cells and (b) DZNU-Bm cell line treated with 50 μg/mL of NiO NPs for 1 h showing the whole distortion of cytoplasm with lyses of cells.

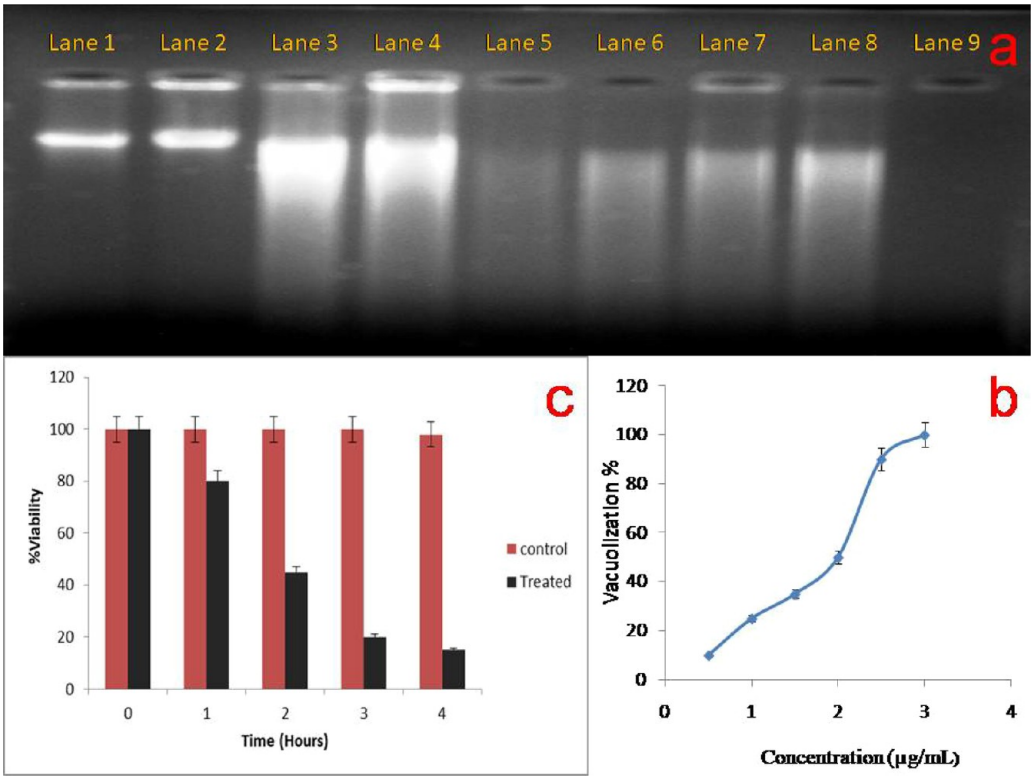

Figure 11. (a) Singlet oxygen mediated DNA degradation by NiO NPs: lane 1: control DNA; lane 2: DNA + supernatant; lane: 3 DNA + 25 μg (NiO + DMSO); lane 4: DNA+ 4 mM sodium citrate; lane 5: DNA + 50 μg NiO; lane 6: DNA + 100 μg NiO; lane 7: DNA + 200 μg NiO; lane 8: DNA + 300 μg NiO; lane 9: DNA + 400 μg NiO (for 2 h at 37 °C in phosphate buffer saline (PBS) maintained at pH 7.5). (b) Effect of different concentrations of NiO NPs on vacuolizaiton in Bm-17 cells under an inverted tissue culture microscope and (c) effect of NiO NPs on the viability of Bm-17 cells. Percent inhibition in growth was quantified based on trypan blue dye exclusion assay at different times.

using NiO NPs. The cells were treated with different concentrations of NiO NPs and were observed to be shrunk and broken (Figure 13c−e), while control liver cells show fresh, healthy, and hepatic parenchyma seen with very distinct nuclei (Figure 13b). The treated cells were expanded and rectangular in shape because of more vacuolization formation in the cells. The cells treated with 1 mg/L of NiO NPs were not affected severely; however, treatment with 30 and 90 mg/L of NiO NPs resulted in dark and shrunken hepatic parenchyma that indicated the disintegration and disappearance of the cells. At a high concentration of nanoparticles, the cytoplasm breaks and forms a striping arrangement. Moreover, the sap between cells becomes very large because these cells expands and breaks. Figure 13d shows the local congestion in the hepatic parenchyma and maximum cell lyses due to more vacuole formation.

Results from Figure 14 show that the SOD values were found to be higher in treated fishes as compared to controls; these suggested that there were significant increases in superoxide dismutase activity that lead to cell damages. Moreover, oxidative stress may be one of the mechanisms underlying NPs-mediated toxicity. Oxidative stress causes a

https://doi.org/10.1021/acsomega.1c06544
ACS Omega 2022, 7, 6869−6884

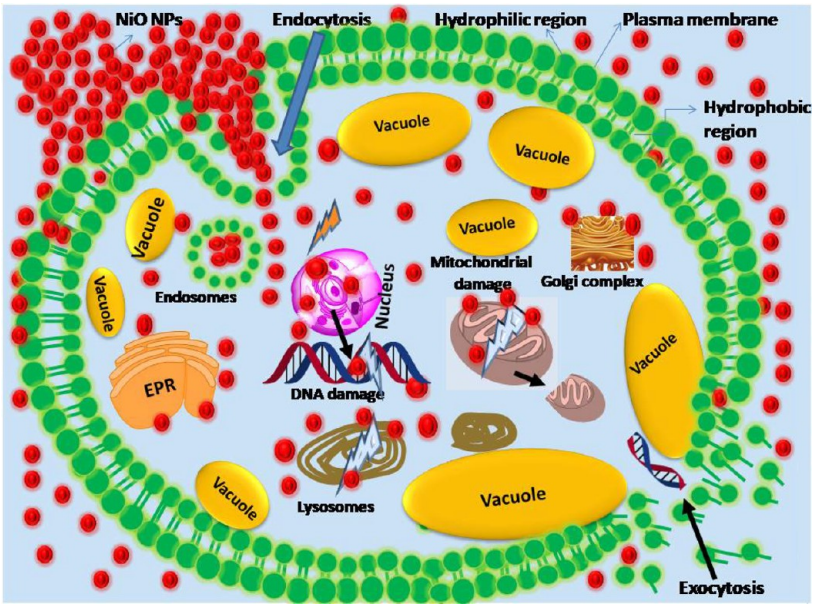

Figure 12. A plausible mechanism of cell lyses due to vacuole formation by NiO NPs.

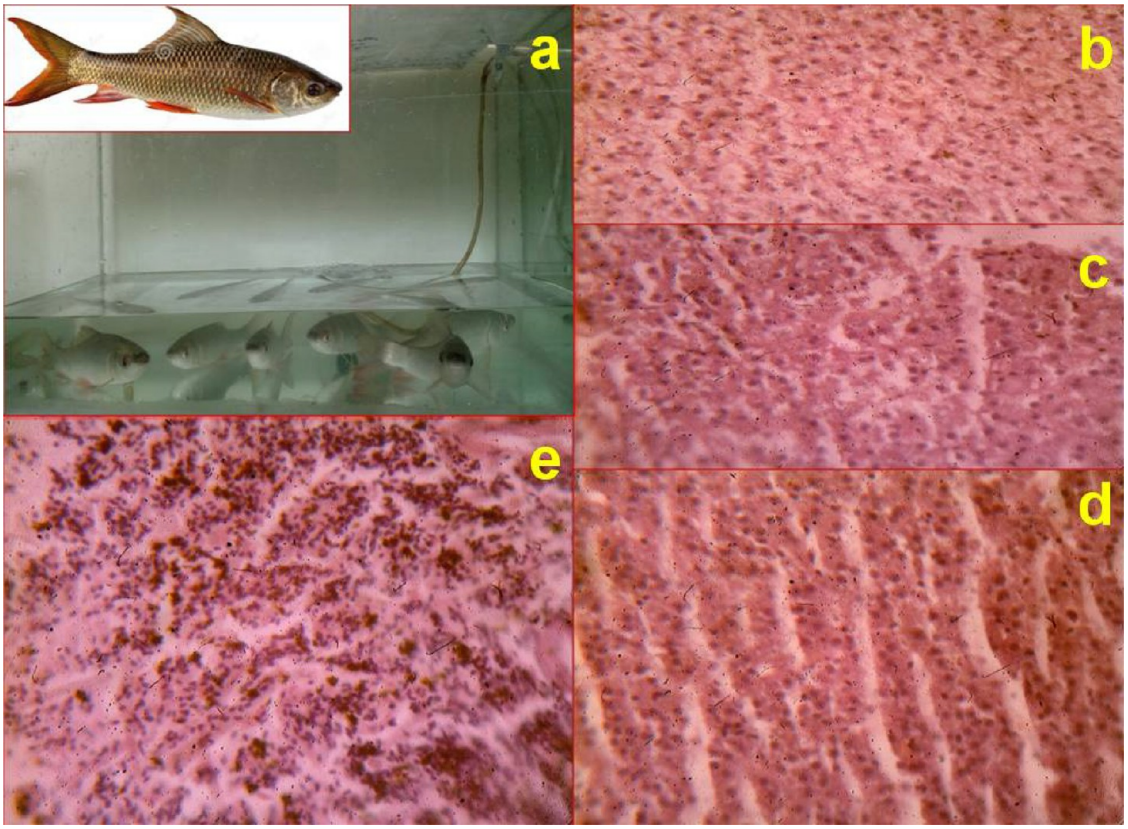

Figure 13. (a) *L. rohita* fish and (b) control. Effect of different concentrations of NiO NPs on liver cells of *L. rohita* fish: (c) 1 mg/L, (d) 30 mg/L, and (e) 90 mg/L.

wide variety of physiological and cellular events including stress, inflammation, and DNA damage.[79] In general, an increase in the activities of both these enzymes was observed in all the tested cell lines when exposed to NiO NPs. The generation of free radicals such as peroxide, superoxide, and hydroxyl ions by NiO NPs was reported to exert lipid peroxidation and damage membrane integrity.

CONCLUSIONS

In conclusion, the present study demonstrated a novel *Cleome simplicifolia*-mediated green synthesis of NiO NPs, and synthesized bioinspired NiO NPs were characterized. XRD revealed a crystalline face-centered-cubic structure. FTIR, UV-DRS, Raman, and XPS spectroscopy confirmed NiO formation. The chemical composition was confirmed by XPS and EDS. BET revealed a mesoporous nature, while SEM and

https://doi.org/10.1021/acsomega.1c06544
ACS Omega 2022, 7, 6869−6884

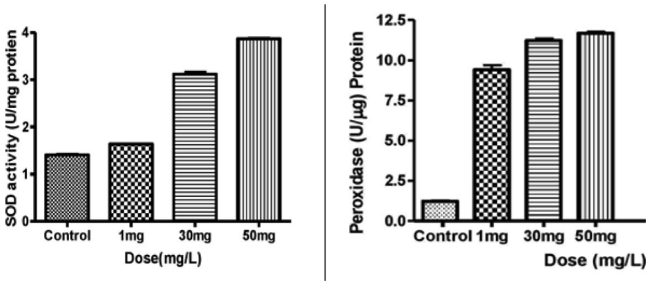

Figure 14. The SOD and peroxidase activities for the elucidation of the toxicity on liver cells of *L. rohita*.

TEM revealed a nanosphere structure with a diameter size of 97 nm, which was formed due to the congregation of 5 and 10 nm average nanoparticles. Moreover, SEM and AFM exploration revealed the nearly monodispersed nature of NiO NPs. Further, the molecular docking study estimated docking energy to be about −9.65284 kcal/mol. Hence, the present study advocated that bioinspired NiO NPs are more effective to explore their toxicity toward binding with genetic molecules. An enhanced cytotoxicity influence of synthesized NiO NPs was explored on the Bm-17 cells of *Bombyx mori* and liver cells of *Labeo rohita* fish. The lyses of Bm-17 cells were additionally investigated by the DNA degradation technique, while liver cells of *Labeo rohita* fishes were probed by the SOD method. An extreme influence of NiO NPs was assessed on cell proliferation at a different dose of concentration. The Bm-17 cells that were treated with 3 μg/mL NiO NPs for 240 min showed an enhanced effect of toxicity; however, when the cells were treated with 50 μg/mL, quick death of cells was observed due to the more vacuole formation in the cells. Noteworthily, it was revealed that if the concentration of NiO NPs increases at the micro-level, unexpected cell lyses occurred. Furthermore, when the liver cells of *Labeo rohita* fishes were treated with 1 mg/L of NiO NPs, toxicity was not observed; however, when the concentration was 30 and 90 mg/L, dark and shrunken hepatic parenchyma was observed. Hence, the main culprit of the cell lyses was more vacuolization in the cells, which was formed by the fusion of NiO NPs with the membrane vesicles during the endocytosis. Thus, the result suggested that the cytotoxicity induced by NiO NPs could be used in anticancer drugs.

EXPERIMENTAL SECTION

Materials and General Methods. *Materials.* Nickel nitrate hexahydrate ($Ni(NO_3)_2{\cdot}6H_2O$) was procured from Himedia Laboratories Ltd., India. Leaves of *Cleome simplicifolia* plant were collected from the Nagpur district area. The cell line of DZNU-Bm-17 cells and fresh liver cells of *L. rohita* fishes were used to check the *in vitro* toxic effect of bioinspired NiO NPs.

Preparation of the Plant Extract. The plant extract was prepared as per the earlier method reported with slight modifications.[80] Initially, plant leaves were washed several times with distilled water to remove the dust. The leaves of the *Cleome simplicifolia* plant were shade dried for 3 days and then machine-ground into a fine powder. Then in a 250 mL conical flask, 10 g of leaf powder was soaked in 150 mL of deionized water; further, the crude mixture was stirred on the hot-magnetic stirrer keeping a constant temperature of 40 °C for 10 min. Finally, the plant extract was continuously centrifuged at 4000 rpm for 10 min to separate plant debris, and it was stored at 4 °C for further experiments.

Cleome simplicifolia-Mediated Green Synthesis of NiO NPs. In a typical synthesis of NiO NPs, 30 mL of leaf extract of *Cleome simplicifolia* (CS) was mixed with 100 mL of 0.1 mM $Ni(NO_3)_2{\cdot}6H_2O$ in a beaker and stirred continuously on a magnetic stirrer at a constant 1080 rpm for 3 h, with strict monitoring of the mixture color every hour. The formation of NiO colloidal dispersion was deduced when the color changed from greenish to reddish-black. Further, the mixture was filtered and centrifuged at 4000 rpm for 30 min; the obtained solid was washed several times with ethanol and acetone to remove impurities. Then the as-obtained solid material was calcined in a muffle furnace at 800 °C to remove impurities, and finally, black NiO NPs were obtained (Figure 15).

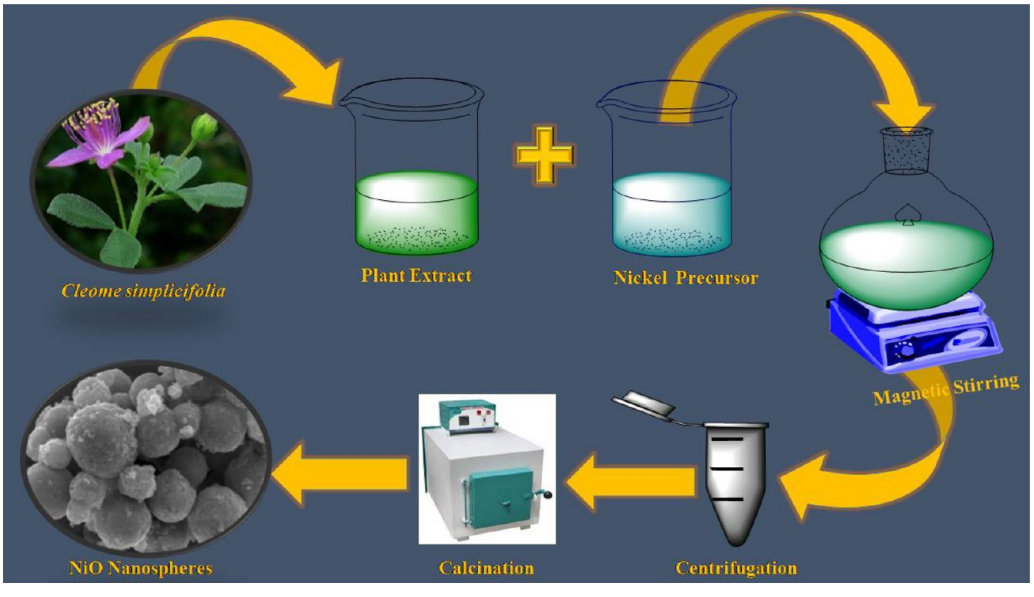

Figure 15. Schematic illustration of the *Cleome simplicifolia*-mediated synthesis of NiO NPs.

https://doi.org/10.1021/acsomega.1c06544
ACS Omega 2022, 7, 6869−6884

B. mori Cell Culture Preparation. DZNU-Bm-17 cells were isolated from the ovarian cell of *B. mori* and maintained at the Center for Sericulture and Biological Research (CSBR), Rashtrasant Tukadoji Maharaj Nagpur University, Nagpur, according to the previously described method.[55] It is the cell line (DZNU-Bm-17 cells) of the silk moth insect; therefore, ethical committee permission was not taken as it is not part of any animal related experiment or human tissue/organ samples. Several primary cultures were set up using 10−15 female larvae for each culture. The primary cultures initiated in the MGM-448 medium were later maintained in a half MGM-448 and half TNM-FH (supplemented with 10% FBS) medium by replenishment once per week.

Passaging. Primary cultures with proliferating cells were suspended using a flushing medium over the monolayer with a Pasteur pipette, and the cells were split into two flasks. The cells were passaged routinely with a split ratio of 1:2 using culture flasks.

Growth Analysis. Primary cultures with proliferating cells were suspended by a flushing medium over the monolayer with a Pasteur pipette, and the cells were split into two flasks. The growth rate of the cells in MGM-448 and TNM-FH media was analyzed by seeding each culture flask with 4.5×10^5 and 5.5×10^5 cells/mL in the respective medium. On alternate days, the cell suspension was sampled from the two culture flasks, and the cell number was counted using a hemocytometer. Viability was determined by trypan blue stain.

In Vitro Cytotoxicity: MTT Assay. The effects of different concentrations (0.5 to 3.0 μg/mL) of NiO NPs were examined on Bm-17 cells using the MTT assay. Initially, 4×10^3 cells were seeded into each well containing 200 μL of the cell culture medium in well plates and incubated for 24 and 48 h. The control experiments were maintained under a similar condition without the addition of the NiO NPs. MTT (100 μL of 5 mg/mL) was added to each well and incubated at 37 °C for 4 h. The dark blue crystals were dissolved by adding 1000 μL of 0.04 M HCl/isopropanol, and after overnight incubation in the dark, the optical density (OD) was measured at a wavelength of 570 nm using a spectrophotometer (ELICO SL-177). The OD values of the experiment were divided by those of the untreated control, and results were presented as the percentage cell viability.

Morphological Assay of Cells Treated with NiO NPs. About 5×10^5 Bm-17 cells of *B. mori* in the culture flask were treated with 0.5, 1.0, 1.5, 2.0, and 3.0 μg/mL concentrations of NiO NPs, and the cell culture was incubated for 24 h at 28 °C. After the treatment, cells were observed under a phase contrast microscope (Vision Plus-5000-PCT, Metzer, India).

Trypan Blue Exclusion Assay. The cell morphology and viability were assessed by the trypan blue dye exclusion assay.[81] The cells were trypsinized with the 0.25% trypsin−EDTA solution, resuspended in the PBS buffer, and stained with the 0.4% trypan blue dye solution (v/v in PBS). Within 2 min, the cells were loaded on the hemocytometer Neubauer chamber, and the numbers of viable and non-viable cells per 1 × 1 mm square were counted under a phase contrast microscope. The dead cells lost the semi-permeability of the membrane, retained the blue dye, and hence were colored, whereas viable or live cells that remained unstained were counted. The % cell viability was determined as [{no. of viable cells/(total no. of viable + non-viable cells)} × 100].

DNA Damage Study. The genomic DNA from the cell line was isolated using the standard protocol.[82] After treatment with 2 μg/mL of NiO NPs for 6−24 h, cells were collected, washed with PBS, and lysed with a solution containing the extraction buffer (100 mM Tris-HC1, pH 8.0, 50 mM NaCl, 50 mM EDTA, and 1% SDS) and Proteinase K (100 μg/mL) was added to the ground tissue and incubated at 37 °C for 2 h with occasional swirling. The DNA was extracted twice with phenol−chloroform−isoamylalcohol (24:24:1) and once with chloroform. The supernatant containing DNA was precipitated using ethanol, resuspended in the TE (10 mM Tris-HCI, 1 mM EDTA, pH 8.0) buffer, and incubated at 37 °C for 1 h after the addition of RNAase (100 mg/mL). DNA was re-extracted using phenol−chloroform and ethanol and precipitated as described earlier. The genomic DNA was quantified on 0.8% agarose gels. The cell line genomic DNA was treated with NiO NPs using increasing concentrations of 0.5 to 2 μg/mL for 120 min at 37 °C in the phosphate buffer saline (PBS) maintained at pH 7.4. Copper sulfate, sodium citrate, and the supernatant of NiO NPs were also incubated along with DNA as control.

Ligand Inhibitor and Receptor Enzyme for Docking Investigation. In the present docking study, biosynthesized NiO NPs were used as ligand inhibitors. The NiO NPs are the replacement of 4-hydroxy-3-nitro-5-({[4-(trifluoromethyl) phenyl]carbamoyl}amino)benzene-1-sulfonamide for the inhibition of enzyme, *i.e.,* PDB ID 6EDA. The presently reported NiO NP ligand is also an effective inhibitor for PDB ID 6EDA. The 2D and 3D structures of NiO NPs (nanosphere NiO NPs) were designed using ChemOffice software 12. The process of 2D and 3D design is elaborately explained by ChemOffice without any modification. The finalized 3D structures of the ligand (nanosphere NiO NPs) were tested for global minima by ascertaining the minimum energy values of the molecule that were calculated as −9.65284 kcal/mol. The present target enzyme is PDB ID 6EDA. The enzyme structure is unique, having various active sites. Kollman charges were assigned and solvation parameters were added to the final macromolecule structure using the Addsol utility of AutoDock-20, 21, 22. The place of the natural inhibitor in the enzyme was selected as the active site of the enzyme for the docking process to interact with the ligand (nanosphere NiO NPs) with the receptor site of the enzyme. Autodock 20, 21 was used to study the interactions of the ligand with the selected protein PDB ID 6EDA. To perform docking, grid designed tools with Autodock were used. At *x*, *y*, and *z* axis as 17.386544, 24.897425, and 23.536096 (Table 4).

Table 4. The Docking Grid Preparation and its Parameters

docking grid preparation	parameters
grid resolution	0.4
converged when RMSD population fitness	<1 kcal/mol
the total memory required for grids	17,971,200 bytes
van der Waals coefficient	−0.00096
hydrogen bond coefficient neutral−neutral	−0.38
the grid prepared and calculated possible interactions	15,627,372 of 722,649,600 total
total memory required for bump grid	835,584 bytes
grid min (*x*, *y*, *z*)	−14.3296, −101,456, 3.62814.
grid max(*x*, *y*, *z*)	3.29539, 14.9794, 27.2531
total memory required for fine grid	835,584 bytes
total memory required for first coarse grid	280 bytes

https://doi.org/10.1021/acsomega.1c06544
ACS Omega 2022, 7, 6869−6884

Docking was performed using both genetic (GA) and non-genetic (non-GA) algorithm techniques. The genetic algorithm is a newly adopted conformational search technique and provides very accurate and quality results in a very short duration of simulation time. The controlled parameter and settings, which were used for docking, are listed in Table 4.

$$\Delta G_{bind} = \Delta G_{vdw} + \Delta G_{hydrophobic} + \Delta GH_{-bond} + \Delta GH_{-bond(chg)} + \Delta G_{deformation} + \Delta G_{o}$$

The obtained results of binding energy for non-GA and GA docking for each set of experiments are listed in Table 4. The negative values of binding energies favor the interaction between the ligand and enzyme.

Toxicity in Liver Cells of Labeo rohita. The fingerling *Labeo rohita* fishes (commonly called as Rohu fish) were obtained from the College of Fishery Science, which is affiliated to Maharashtra Animal and Fishery Science University, Nagpur, and transported in well-aerated condition to the Department of Zoology, Seth Kesarimal Porwal College, Kamptee. Rohu fish is extensively utilized in aquaculture and is a common food; therefore, ethical committee permission was not taken as it is not part of any animal related experiment or human tissue/organ samples. Further, fishes were kept for a week in an aquarium to acclimatize to the laboratory environment. During this period, they were fed four times a day at 10 a.m., 12 p.m., 2 p.m., and 4 p.m. by commercial pellets (28% protein). Next, different concentration doses of biosynthesized NiO NPs were administered in each aquarium except the control aquarium. After 15 days, the experiments were performed to check the toxicity of NiO NPs on the liver organ. Therefore, the fishes were utilized for the experiment by giving chloroform doses, and their length and weight were recorded during the experiment. The liver of fishes was dissected and kept in 10% formalin. Tissues fixed in 10% formalin were washed in running tap water. The tissues were dehydrated by passing through a graded series of ethyl alcohol, cleaned in xylol, and embedded in paraffin wax (58 to 60 °C). The sections were cut at a thickness of 4 to 6 μm with the help of a rotary microtome (Leica RM 2145). Further, for the histological study, the liver section was stained with hematoxylin−eosin. The photomicrographs were taken with a 35 mm Leica camera attached to a microscope and enlarged to the required size. All microscopic measurements were taken with the help of an eyepiece micrometer calibrated to a stage micrometer scale. The fish liver was removed and weighed by a Shimadzu electronic weighing balance.

AUTHOR INFORMATION

Corresponding Authors

Alok R. Rai − *Post Graduate Department of Microbiology, Seth Kesarimal Porwal College of Arts and Science and Commerce, Kamptee 441001, India*; Email: alok.rrai@gmail.com

Ratiram G. Chaudhary − *Post Graduate Department of Chemistry, Seth Kesarimal Porwal College of Arts and Science and Commerce, Kamptee 441001, India*; orcid.org/0000-0002-7874-585X; Email: chaudhary_rati@yahoo.com

Dhanraj T. Masram − *Department of Chemistry, University of Delhi, Delhi 110007, India*; orcid.org/0000-0001-6273-8199; Email: dhanraj_masram27@rediffmail.com

Authors

Prashant B. Chouke − *Post Graduate Department of Chemistry, Seth Kesarimal Porwal College of Arts and Science and Commerce, Kamptee 441001, India*

Ajay K. Potbhare − *Post Graduate Department of Chemistry, Seth Kesarimal Porwal College of Arts and Science and Commerce, Kamptee 441001, India*

Nitin P. Meshram − *Department of Zoology, Seth Kesarimal Porwal College of Arts and Science and Commerce, Kamptee 441001, India*

Manoj M. Rai − *Centre for Sericulture & Biological Research Institute, R.T.M. Nagpur University, Nagpur 440033, India*

Kanhaiya M. Dadure − *Department of Chemistry, J.B. Science College, Wardha 442001, India*

Karan Chaudhary − *Department of Chemistry, University of Delhi, Delhi 110007, India*

Martin F. Desimone − *Universidad de Buenos Aires, Consejo Nacional de Investigaciones Científicas y Técnicas (CONICET), Instituto de Química y Metabolismo del Fármaco (IQUIMEFA), Facultad de Farmacia y Bioquímica, Buenos Aires 1113, Argentina*; orcid.org/0000-0002-0571-7962

Complete contact information is available at: https://pubs.acs.org/10.1021/acsomega.1c06544

Author Contributions

R.G. Chaudhary/A.R. Rai: conceptualization/methodology/supervision; P.B. Chouke/A.K. Potbhare/N.P. Meshram/M.M. Rai: original draft preparation/data curation/investigation/validation/formal analysis; R.G. Chaudhary/Martin Desimone/D.T. Masram/K. Chaudhary: visualization/writing of paper/reviewing and editing/interpretation of characterization; K.M. Dadure/R.G. Chaudhary: docking study/interpretation.

Notes

The authors declare no competing financial interest.

ACKNOWLEDGMENTS

The authors are grateful to the Principal, Seth Kesarimal Porwal College, Kamptee, India, for providing the necessary research facilities for the studies. We are also thankful to the Centre for Sericulture & Biological Research Institute, R.T.M. Nagpur University, Nagpur, for cell line research facilities. We are also grateful to Dr. Javed G. Khan Pathan, Assistant Professor & Head, Department of Aquatic Environment Management, College of Fishery Science, Nagpur, for supplying fingerling fishes.

REFERENCES

(1) Bhattacharya, P.; Du, D.; Lin, Y. Bioinspired Nanoscale Materials for Biomedical and Energy Applications. *J. R. Soc., Interface* **2014**, *11*, 20131067.

(2) Iravani, S.; Varma, R. S. Bacteria in Heavy Metal Remediation and Nanoparticle Biosynthesis. *ACS Sustainable Chem. Eng.* **2020**, *8*, 5395−5409.

(3) Ayangbenro, A.; Babalola, O. A New Strategy for Heavy Metal Polluted Environments: A Review of Microbial Biosorbents. *Int. J. Environ. Res. Public Health* **2017**, *14*, 94.

(4) Suganthi, P.; Murali, M.; Athif, P.; Sadiq Bukhari, A.; Syed Mohamed, H. E.; Basu, H.; Singhal, R. K. Haemato-Immunological Studies in ZnO and TiO_2 Nanoparticles Exposed Euryhaline Fish, Oreochromis Mossambicus. *Environ. Toxicol. Pharmacol.* **2019**, *66*, 55−61.

(5) Ma, H.; Williams, P. L.; Diamond, S. A. Ecotoxicity of Manufactured ZnO Nanoparticles - A Review. *Environ. Pollut.* **2013**, *172*, 76−85.
(6) Bondarenko, O.; Juganson, K.; Ivask, A.; Kasemets, K.; Mortimer, M.; Kahru, A. Toxicity of Ag, CuO and ZnO Nanoparticles to Selected Environmentally Relevant Test Organisms and Mammalian Cells in Vitro: A Critical Review. *Arch. Toxicol.* **2013**, *87*, 1181−1200.
(7) Abbas, S. H.; Ismail, I. M.; Mostafa, T. M.; Sulaymon, A. H. Biosorption of Heavy Metals: A Review. *J. Chem. Sci. Technol.* **2014**, *3*, 74−102.
(8) Brunner, T. J.; Wick, P.; Manser, P.; Spohn, P.; Grass, R. N.; Limbach, L. K.; Bruinink, A.; Stark, W. J. In Vitro Cytotoxicity of Oxide Nanoparticles: Comparison to Asbestos, Silica, and the Effect of Particle Solubility. *Environ. Sci. Technol.* **2006**, *40*, 4374−4381.
(9) Maleki, P.; Nemati, F.; Gholoobi, A.; Hashemzadeh, A.; Sabouri, Z.; Darroudi, M. Green facile synthesis of silver-doped cerium oxide nanoparticles and investigation of their cytotoxicity and antibacterial activity. *Inorg. Chem. Commun.* **2021**, *131*, 108762.
(10) Chaudhary, K.; Subodh; Prakash, K.; Mogha, N. K.; Masram, D. T. Fruit Waste (Pulp) Decorated CuO NFs as Promising Platform for Enhanced Catalytic Response and Its Peroxidase Mimics Evaluation. *Arab. J. Chem* **2020**, *13*, 4869−4881.
(11) Chaudhary, K.; Kumar, K.; Venkatesu, P.; Masram, D. T. In-Depth Understanding of a Nano-Bio Interface between Lysozyme and Au NP-Immobilized N-Doped Reduced Graphene Oxide 2-D Scaffolds. *Nanoscale Adv.* **2020**, *2*, 2146−2159.
(12) Chaudhary, K.; Masram, D. T. Biological Activities of Nanoparticles and Mechanism of Action. In *Model Organisms to Study Biological Activities and Toxicity of Nanoparticles*; Springer, Singapore, 2020; pp. 19−34.
(13) Subodh; Mogha, N. K.; Chaudhary, K.; Kumar, G.; Masram, D. T. Fur-Imine-Functionalized Graphene Oxide-Immobilized Copper Oxide Nanoparticle Catalyst for the Synthesis of Xanthene Derivatives. *ACS Omega* **2018**, *3*, 16377−16385.
(14) Xia, T.; Kovochich, M.; Liong, M.; Mädler, L.; Gilbert, B.; Shi, H.; Yeh, J. I.; Zink, J. I.; Nel, A. E. Comparison of the Mechanism of Toxicity of Zinc Oxide and Cerium Oxide Nanoparticles Based on Dissolution and Oxidative Stress Properties. *ACS Nano* **2008**, *2*, 2121−2134.
(15) Sabouri, Z.; Sabouri, M.; Amiri, M.S.; Khatami, M.; Darroudi, M. Plant-based synthesis of cerium oxide nanoparticles using Rheum turkestanicum extract and evaluation of their cytotoxicity and photocatalytic properties. In *Materials Technology*; Advanced Performance Materials, 2020.
(16) Muralisankar, T.; Saravana Bhavan, P.; Radhakrishnan, S.; Seenivasan, C.; Srinivasan, V. The Effect of Copper Nanoparticles Supplementation on Freshwater Prawn Macrobrachium Rosenbergii Post Larvae. *J. Trace Elem. Med. Biol.* **2016**, *34*, 39−49.
(17) Clearwater, S. J.; Farag, A. M.; Meyer, J. S. Bioavailability and Toxicity of Dietborne Copper and Zinc to Fish. *Comp. Biochem. Physiol., Part C: Toxicol. Pharmacol.* **2002**, *132*, 269−313.
(18) Abbasi, B. A.; Iqbal, J.; Mahmood, T.; Ahmad, R.; Kanwal, S.; Afridi, S. Plant-mediated synthesis of nickel oxide nanoparticles (NiO) via *Geranium wallichianum*: Characterization and different biological applications. *Mater. Res. Express* **2019**, *6*, No. 0850a7.
(19) Iqbal, J.; Abbasi, B. A.; Ahmad, R.; Mahmoodi, M.; Munir, A.; Zahra, S. A.; Capasso, R. Phytogenic synthesis of nickel oxide nanoparticles (NiO) using fresh leaves extract of Rhamnus triquetra (wall.) and investigation of its multiple in vitro biological potentials. *Biomedicines* **2020**, *8*, 117.
(20) Iqbal, J.; Abbasi, B. A.; Mahmood, T.; Hameed, S.; Munir, A.; Kanwal, S. Green synthesis and characterizations of Nickel oxide nanoparticles using leaf extract of Rhamnus virgata and their potential biological applications. *Appl. Organomet. Chem.* **2019**, *33*, No. e4950.
(21) Uddin, S.; Safdar, L. B.; Iqbal, J.; Yaseen, T.; Laila, S.; Anwar, S.; Quraishi, U. M. Green synthesis of nickel oxide nanoparticles using leaf extract of *Berberis balochistanica*: Characterization, and diverse biological applications. *Microsc. Res. Tech.* **2021**, *84*, 2004−2016.
(22) Din, M. I.; Tariq, M.; Hussain, Z.; Khalid, R. Single step green synthesis of nickel and nickel oxide nanoparticles from *Hordeum vulgare* for photocatalytic degradation of methylene blue dye. *Inorg. Nano-Met. Chem.* **2020**, *50*, 292−297.
(23) Sabouri, Z.; Akbari, A.; Hosseini, H. A.; Khatami, M.; Darroudi, M. Tragacanth-mediate synthesis of NiO nanosheets for cytotoxicity and photocatalytic degradation of organic dyes. *Bioprocess Biosyst. Eng.* **2020**, *43*, 1209−1218.
(24) Mirza, A. U.; Khan, M. S.; Kareem, A.; Nami, S. A.; Bhat, S. A.; Mohammad, A.; Nishat, N. Biomediated synthesis, characterization, and biological applications of nickel oxide nanoparticles derived from Toona ciliata, Ficus carica and Pinus roxburghii. *Bioprocess Biosyst. Eng.* **2021**, *44*, 1461−1476.
(25) Ali, T.; Warsi, M. F.; Zulfiqar, S.; Sami, A.; Ullah, S.; Rasheed, A.; Baig, M. M. Green nickel/nickel oxide nanoparticles for prospective antibacterial and environmental remediation applications. *Ceram. Int.* **2021**, DOI: 10.1016/j.ceramint.2021.12.039.
(26) Yuvakkumar, R.; Suresh, J.; Nathanael, A. J.; Sundrarajan, M.; Hong, S. I. Rambutan (*Nephelium lappaceum* L.) peel extract assisted biomimetic synthesis of nickel oxide nanocrystals. *Mater. Lett.* **2014**, *128*, 170−174.
(27) Ghazal, S.; Khandannasab, N.; Hosseini, H. A.; Sabouri, Z.; Rangrazi, A.; Darroudi, M. Green synthesis of copper-doped nickel oxide nanoparticles using okra plant extract for the evaluation of their cytotoxicity and photocatalytic properties. *Ceram. Int.* **2021**, *47*, 27165−27176.
(28) Haider, A.; Ijaz, M.; Ali, S.; Haider, J.; Imran, M.; Majeed, H.; Ikram, M. Green synthesized phytochemically (Zingiber officinale and Allium sativum) reduced nickel oxide nanoparticles confirmed bactericidal and catalytic potential. *Nanoscale Res. Lett.* **2020**, *15*, 1−11.
(29) Thema, F. T.; Manikandan, E.; Gurib-Fakim, A.; Maaza, M. Single phase Bunsenite NiO nanoparticles green synthesis by *Agathosma betulina* natural extract. *J. Alloys Compd.* **2016**, *657*, 655−661.
(30) Sabouri, Z.; Akbari, A.; Hosseini, H. A.; Khatami, M.; Darroudi, M. Green-based bio-synthesis of nickel oxide nanoparticles in *Arabic gum* and examination of their cytotoxicity, photocatalytic and antibacterial effects. *Green Chem. Lett. Rev.* **2021**, *14*, 404−414.
(31) Ezhilarasi, A. A.; Vijaya, J. J.; Kaviyarasu, K.; Kennedy, L. J.; Ramalingam, R. J.; Al-Lohedan, H. A. Green synthesis of NiO nanoparticles using *Aegle marmelos* leaf extract for the evaluation of *in-vitro* cytotoxicity, antibacterial and photocatalytic properties. *J. Photochem. Photobiol. B* **2018**, *180*, 39−50.
(32) Chaudhary, R. G.; Chouke, P. B.; Bagade, R. D.; Potbhare, A. K.; Dadure, K. M. Molecular Docking and Antioxidant Activity of *Cleome simplicifolia* Assisted Synthesis of Cerium Oxide Nanoparticles. *Mater. Today: Procs* **2020**, *29*, 1085.
(33) Umekar, M. S.; Bhusari, G. S.; Potbhare, A. K.; Chaudhary, R. G. ZnO Decorated Reduced Graphene Oxide Nanohybrid by *Clerodendrum Infortunatum*. *Emer. Mater Res.* **2021**, *10*, 75−84.
(34) Umekar, M. S.; Bhusari, G. S.; Potbhare, A. K.; Mondal, A.; Kapgate, B. P.; Desimone, M. F.; Chaudhary, R. G. Bioinspired reduced graphene oxide based nanohybrids for photocatalysis and antibacterial applications. *Curr. Pharm. Biotechnol.* **2021**, *22*, 1759−1781.
(35) Chaudhary, R. G.; Potbhare, A. K.; Tarik Aziz, S. K.; Umekar, M. S.; Bhuyar, S. S.; Mondal, A. Phytochemically fabricated reduced graphene Oxide-ZnO NCs by *Sesbania bispinosa* for photocatalytic performances. *Mater. Today:Procs* **2021**, *36*, 756−762.
(36) Oukarroum, A.; Barhoumi, L.; Samadani, M.; Dewez, D. Toxic Effects of Nickel Oxide Bulk and Nanoparticles on the Aquatic Plant Lemna Gibba L. *Biomed Res. Int.* **2015**, *2015*, 1.
(37) Oyabu, T.; Ogami, A.; Morimoto, Y.; Shimada, M.; Lenggoro, W.; Okuyama, K.; Tanaka, I. Biopersistence of Inhaled Nickel Oxide Nanoparticles in Rat Lung. *Inhalation Toxicol.* **2007**, *19*, 55−58.
(38) Manna, I.; Bandyopadhyay, M. Engineered Nickel Oxide Nanoparticle Causes Substantial Physicochemical Perturbation in Plants. *Front. Chem.* **2017**, *5*, 92.

https://doi.org/10.1021/acsomega.1c06544
ACS Omega 2022, 7, 6869−6884

(39) Nie, J.; Pan, Y.; Shi, J.; Guo, Y.; Yan, Z.; Duan, X.; Xu, M. A Comparative Study on the Uptake and Toxicity of Nickel Added in the Form of Different Salts to Maize Seedlings. *Int. J. Environ. Res. Public Health* **2015**, *12*, 15075−15087.
(40) Horie, M.; Fukui, H.; Nishio, K.; Endoh, S.; Kato, H.; Fujita, K.; Miyauchi, A.; Nakamura, A.; Shichiri, M.; Ishida, N.; Kinugasa, S.; Morimoto, Y.; Niki, E.; Yoshida, Y.; Iwahashi, H. Evaluation of Acute Oxidative Stress Induced by NiO Nanoparticles in Vivo and in Vitro. *J. Occup. Health* **2011**, *53*, 64−74.
(41) Sousa, C. A.; Soares, H. M. V. M.; Soares, E. V. Toxic Effects of Nickel Oxide (NiO) Nanoparticles on the Freshwater Alga Pseudokirchneriella Subcapitata. *Aquat. Toxicol.* **2018**, *204*, 80−90.
(42) Baek, Y. W.; An, Y. J. Microbial Toxicity of Metal Oxide Nanoparticles (CuO, NiO, ZnO, and Sb_2O_3) to Escherichia Coli, Bacillus Subtilis, and Streptococcus Aureus. *Sci. Total Environ.* **2011**, *409*, 1603−1608.
(43) Lu, S.; Duffin, R.; Poland, C.; Daly, P.; Murphy, F.; Drost, E.; MacNee, W.; Stone, V.; Donaldson, K. Efficacy of Simple Short-Term in Vitro Assays for Predicting the Potential of Metal Oxide Nanoparticles to Cause Pulmonary Inflammation. *Environ. Health Perspect.* **2009**, *117*, 241−247.
(44) Pietruska, J. R.; Liu, X.; Smith, A.; McNeil, K.; Weston, P.; Zhitkovich, A.; Hurt, R.; Kane, A. B. Bioavailability, Intracellular Mobilization of Nickel, and HIF-1α Activation in Human Lung Epithelial Cells Exposed to Metallic Nickel and Nickel Oxide Nanoparticles. *Toxicol. Sci.* **2011**, *124*, 138−148.
(45) Ahamed, M.; Ali, D.; Alhadlaq, H. A.; Akhtar, M. J. Nickel Oxide Nanoparticles Exert Cytotoxicity via Oxidative Stress and Induce Apoptotic Response in Human Liver Cells (HepG2). *Chemosphere* **2013**, *93*, 2514−2522.
(46) Ogami, A.; Morimoto, Y.; Myojo, T.; Oyabu, T.; Murakami, M.; Todoroki, M.; Nishi, K.; Kadoya, C.; Yamamoto, M.; Tanaka, I. Pathological Features of Different Sizes of Nickel Oxide Following Intratracheal Instillation in Rats. *Inhalation Toxicol.* **2009**, *21*, 812−818.
(47) Morimoto, N.; de León, M. S. P.; Nishimura, T.; Zollikofer, C. P. E. Femoral Morphology and Femoropelvic Musculoskeletal Anatomy of Humans and Great Apes: A Comparative Virtopsy Study. *Anat. Rec.* **2011**, *294*, 1433−1445.
(48) Cao, Z.; Fang, Y.; Lu, Y.; Qian, F.; Ma, Q.; He, M.; Pi, H.; Yu, Z.; Zhou, Z. Exposure to Nickel Oxide Nanoparticles Induces Pulmonary Inflammation through NLRP3 Inflammasome Activation in Rats. *Int. J. Nanomed.* **2016**, *Volume 11*, 3331−3346.
(49) Huang, G.; Zhang, Y.; Zhang, Q.; Zhang, B.; Wen, L. Vacuolization and Apoptosis Induced by Nano-Selenium in HeLa Cell Line. *Sci. China Chem.* **2010**, *53*, 2272−2278.
(50) Nel, A.; Xia, T.; Mädler, L.; Li, N. Toxic Potential of Materials at the Nanolevel. *Science* **2006**, *311*, 622−627.
(51) Kato, T.; Sugioka, S.; Itagaki, K.; Park, E. Y. Gene Transduction in Mammalian Cells Using Bombyx Mori Nucleopolyhedrovirus Assisted by Glycoprotein 64 of Autographa Californica Multiple Nucleopolyhedrovirus. *Sci. Rep.* **2016**, *6*, 1−9.
(52) Kadono-Okuda, K.; Sakurai, H.; Takeda, S.; Okuda, T. Synchronous Growth of a Parasitoid, Perilitus Coccinellae, and Teratocytes with the Development of the Host, Coccinella Septempunctata. *Entomol. Exp. Appl.* **1995**, *75*, 145−149.
(53) Motohashi, T.; Shimojima, T.; Fukagawa, T.; Maenaka, K.; Park, E. Y. Efficient Large-Scale Protein Production of Larvae and Pupae of Silkworm by Bombyx Mori Nuclear Polyhedrosis Virus Bacmid System. *Biochem. Biophys. Res. Commun.* **2005**, *326*, 564−569.
(54) Luckow, V. A. Cloning and Expression of Heterologous Genes in Insect Cells with Baculovirus Vectors. *Recomb. DNA Technol. Appl.* **1991**, 97−152.
(55) Khurad, A. M.; Bahekar, R. S.; Zhang, M. J.; Tiple, A. D.; Lee, J. M.; Zhang, C. X.; Kusakabe, T. Development and Characterization of a New Bombyx Mori Cell Line for Protein Expression. *J. Asia. Pac. Entomol.* **2013**, *16*, 17−22.
(56) Sudeep, A. B.; Mishra, A. C.; Shouche, Y. S.; Pant, U.; Mourya, D. T. Establishment of Two New Cell Lines from Bombyx Mori (L.) (Lepidoptera: Bombycidae) & Their Susceptibility to Baculoviruses. *Indian J. Med. Res.* **2002**, *115*, 189−193.
(57) Zhang, H.; Tian, B.; Xue, J.; Ding, G.; Ji, X.; Cao, Y. Hierarchical Non-Woven Fabric NiO/TiO_2 Film as an Efficient Anode Material for Lithium-Ion Batteries. *RSC Adv.* **2019**, *9*, 24682−24687.
(58) Wu, S.; Hui, K. S.; Hui, K. N.; Yun, J. M.; Kim, K. H. Silver Particle-Loaded Nickel Oxide Nanosheet Arrays on Nickel Foam as Advanced Binder-Free Electrodes for Aqueous Asymmetric Supercapacitors. *RSC Adv.* **2017**, *7*, 41771−41778.
(59) Tanna, J. A.; Chaudhary, R. G.; Gandhare, N. V.; Rai, A. R.; Yerpude, S.; Juneja, H. D. Copper Nanoparticles Catalysed an Efficient One-Pot Multicomponents Synthesis of Chromenes Derivatives and Its Antibacterial Activity. *J. Exp. Nanosci.* **2016**, *11*, 884−900.
(60) Sabouri, Z.; Akbari, A.; Hosseini, H. A.; Darroudi, M. Facile Green Synthesis of NiO Nanoparticles and Investigation of Dye Degradation and Cytotoxicity Effects. *J. Mol. Struct.* **2018**, *1173*, 931−936.
(61) Bhosale, M. A.; Bhanage, B. M. Rapid Synthesis of Nickel Oxide Nanorods and Its Applications in Catalysis. *Adv. Powder Technol.* **2015**, *26*, 422−427.
(62) Potbhare, A. K.; Chauke, P. B.; Zahra, S.; Sonkusare, V.; Bagade, R.; Ummekar, M.; Chaudhary, R. G. Microwave-Mediated Fabrication of Mesoporous Bi-Doped $CuAl_2O_4$ Nanocomposites for Antioxidant and Antibacterial Performances. *Mater. Today Proc.* **2019**, *15*, 454−463.
(63) Sunny, A.; Balasubramanian, K. Plasmon Induced Enhancement of Surface Optical Phonon Modes and Magnon Properties of NiO Nanoparticles: Raman Spectral Probe. *Phys. Chem. Chem. Phys.* **2020**, *22*, 22815−22822.
(64) Asencios, Y. J. O.; Nascente, P. A. P.; Assaf, E. M. Partial Oxidation of Methane on NiO-MgO-ZrO 2 Catalysts. *Fuel* **2012**, *97*, 630−637.
(65) Saravanakumar, S.; Saravanan, R.; Sasikumar, S. Effect of Sintering Temperature on the Magnetic Properties and Charge Density Distribution of Nano-NiO. *Chem. Pap.* **2014**, *68*, 788−797.
(66) Kalaie, M. R.; Youzbashi, A. A.; Meshkot, M. A.; Hosseini-Nasab, F. Preparation and Characterization of Superparamagnetic Nickel Oxide Particles by Chemical Route. *Appl. Nanosci.* **2016**, *6*, 789−795.
(67) Potbhare, A. K.; Chaudhary, R. G.; Chouke, P. B.; Yerpude, S.; Mondal, A.; Sonkusare, V. N.; Rai, A. R.; Juneja, H. D. Phytosynthesis of Nearly Monodisperse CuO Nanospheres Using Phyllanthus Reticulatus/Conyza Bonariensis and Its Antioxidant/Antibacterial Assays. *Mater. Sci. Eng. C* **2019**, *99*, 783−793.
(68) Radhakrishnan, A.; Rejani, P.; Beena, B. Synthesis, Characterization and Antimicrobial Properties of CuO Nanoparticles against Gram-Positive and Gram-Negative Bacterial Strains. *Int. J. Nano Dimens.* **2014**, *5*, 519−524.
(69) Manikandan, A.; Judith Vijaya, J.; John Kennedy, L. Comparative Investigation of NiO Nano- and Microstructures for Structural, Optical and Magnetic Properties. *Phys. E: Low-Dimens. Syst. Nanostructures* **2013**, *49*, 117−123.
(70) Hrenovic, J.; Milenkovic, J.; Daneu, N.; Kepcija, R. M.; Rajic, N. Antimicrobial Activity of Metal Oxide Nanoparticles Supported onto Natural Clinoptilolite. *Chemosphere* **2012**, *88*, 1103−1107.
(71) Bagade, R.; Chaudhary, R. G.; Potbhare, A.; Mondal, A.; Desimone, M.; Dadure, K.; Mishra, R.; Juneja, H. Microspheres/Custard-Apples Copper (II) Chelate Polymer: Characterization, Docking, Antioxidant and Antibacterial Assay. *ChemistrySelect* **2019**, *4*, 6233−6244.
(72) Wilson, W. R.; Hay, M. P. Targeting Hypoxia in Cancer Therapy. *Nat. Rev. Cancer* **2011**, *11*, 393−410.
(73) Taddei, M. L.; Giannoni, E.; Comito, G.; Chiarugi, P. Microenvironment and Tumor Cell Plasticity: An Easy Way Out. *Cancer Lett.* **2013**, *341*, 80−96.
(74) Ahamed, M.; Karns, M.; Goodson, M.; Rowe, J.; Hussain, S. M.; Schlager, J. J.; Hong, Y. DNA Damage Response to Different

https://doi.org/10.1021/acsomega.1c06544
ACS Omega 2022, 7, 6869−6884

Surface Chemistry of Silver Nanoparticles in Mammalian Cells. *Toxicol. Appl. Pharmacol.* **2008**, *233*, 404−410.
(75) Faisal, M.; Saquib, Q.; Alatar, A. A.; Al-Khedhairy, A. A.; Hegazy, A. K.; Musarrat, J. Phytotoxic Hazards of NiO-Nanoparticles in Tomato: A Study on Mechanism of Cell Death. *J. Hazard. Mater.* **2013**, *250-251*, 318−332.
(76) Saquib, Q.; Siddiqui, M. A.; Ahmad, J.; Ansari, S. M.; Faisal, M.; Wahab, R.; Alatar, A. A.; Al-Khedhairy, A. A.; Musarrat, J. Nickel Oxide Nanoparticles Induced Transcriptomic Alterations in HEPG2 Cells. *Adv. Exp. Med. Biol.* **2018**, *1048*, 163−174.
(77) Morissette, G.; Moreau, E.; C.-Gaudreault, R.; Marceau, F. Massive Cell Vacuolization Induced by Organic Amines Such as Procainamide. *J. Pharmacol. Exp. Ther* **2004**, *310*, 395−406.
(78) Stoimenov, P. K.; Klinger, R. L.; Marchin, G. L.; Klabunde, K. J. Metal Oxide Nanoparticles as Bactericidal Agents. *Langmuir* **2002**, *18*, 6679−6686.
(79) AshaRani, P. V.; Mun, G. L. K.; Hande, M. P.; Valiyaveettil, S. Cytotoxicity and Genotoxicity of Silver Nanoparticles in Human Cells. *ACS Nano* **2009**, *3*, 279−290.
(80) Chouke, P. B.; Potbhare, A. K.; Dadure, K. M.; Mungole, A. J.; Meshram, N. P.; Chaudhary, R. R.; Rai, A. R.; Chaudhary, R. G. An Antibacterial Activity of Bauhinia Racemosa Assisted ZnO Nanoparticles during Lunar Eclipse and Docking Assay. *Mater. Today Proc.* **2019**, *29*, 815−821.
(81) Strober, W. Trypan Blue Exclusion Test of Cell Viability. *Curr. Protoc. Immunol.* **2015**, *111*, A3.B.1-A3.B.3.
(82) Nagaraja, G. M.; Nagaraju, J. Genome Fingerprinting of the Silkworm, Bombyx Mori, Using Random Arbitrary Primers. *Electrophoresis* **1995**, *16*, 1633−1638.

https://doi.org/10.1021/acsomega.1c06544
ACS Omega 2022, 7, 6869−6884